Fast Spatially Coherent Fiber Orientation Estimation in Diffusion MRI from kq-Space Sampling

Fast Spatially Coherent Fiber Orientation Estimation in Diffusion MRI from kq-Space Sampling

Marica Pesce*, Audrey Repetti*†, and Yves Wiaux*
*Institute of Sensors, Signals and Systems, Heriot-Watt University, Edinburgh EH14 4AS, United Kingdom
†Department of Actuarial Mathematics & Statistics, Heriot-Watt University, Edinburgh EH14 4AS, United Kingdom

***Abstract*—Diffusion Magnetic Resonance Imaging is a state-of-the-art technique that can provide accurate identification of complex neuronal fiber configurations in the human brain. Typical acquisition times are however too long for the clinical application. We propose a method to recover the fiber orientation distribution (FOD) at high spatio-angular resolution via practical kq-space under-sampling patterns that enable both acceleration and super-resolution. The inverse problem for FOD reconstruction is regularized by a structured sparsity prior promoting simultaneously voxelwise sparsity and spatial smoothness of fiber orientations. A convex minimization problem is formulated and solved via a forward-backward algorithm. Real data analysis suggest that high spatio-angular resolution FOD mapping can be achieved from severe kq-space acceleration.**

***Index Terms*—Diffusion MRI, k-space, q-space, inverse problem, forward-backward algorithm**

I. Introduction

Diffusion Magnetic Resonance Imaging (dMRI) is a powerful tool for studying the tissues micro-structure in-vivo and in a non invasive way. In highly ordered tissues, the random displacements of the water molecules induced by thermal energy are constrained within the compartments composing the tissues. It is on this principle that dMRI infer the configuration and the integrity of the white matter fiber bundles in the brain. The dMRI technique is extensively used in Neuroscience for the study of the neuronal connectivity [1], [2] and in clinics, for the diagnosis of neurodegenerative diseases such as Schizophrenia and Alzheimer's disease [3], [4].

Unlike standard MRI, diffusion weighted (DW) volumes acquired in dMRI are characterized by a signal attenuation which reflects water molecule diffusion. Each DW volume is sensitive to diffusion along a specific direction and intensity, identified by a 3D point $\mathbf{q}$. The associated 3D space is called q-space, and it is defined by the diffusion gradients. DTI is currently the most widely used approach in clinics, since it requires the use of only 6 gradients [5]. However, DTI is unable to distinguish the presence of multiple fibers in the same voxel. Recently, high angular resolution diffusion imaging (HARDI) methods have shown to overcome this limitation. These approaches rely on signals acquired by a large number of diffusion gradients (typically 60-100 gradients). Besides angular resolution, spatial resolution has shown to be necessary for the accurate recovery of the fiber configurations. However, in the everyday clinical practice, such high resolution acquisitions are limited by the long scan times required.

In the last decades, spherical deconvolution (SD) [6], [7] has gained particular attention to estimate complex fiber orientations. This approach consists in solving an inverse problem [8] modeling the HARDI signal as a spherical convolution between the fiber orientation distribution (FOD) representing the few active fiber orientations, and a kernel representing the response signal of a single fiber [6], [7], [9], [10]. Lately, the compressed sensing (CS) theory has promoted the use of SD methods for the FOD recovery from a reduced number of diffusion gradients (called q-space under-sampling) [7], [8], [11]. In parallel, to shorten the acquisition process in MRI, methods considering a reduced number of Fourier samples have extensively been used during the last decades. These methods are named k-space under-sampling approaches [12].

In recent years, many techniques have been developed in order to speed up high resolution dMRI acquisitions. In particular, the recovery of the fiber configurations from incomplete k and q-space samples has recently been proposed. Typically, the sparsity of the fiber coefficients is promoted by minimizing the ℓ_1 norm and the TV penalty acting on the diffusion-weighted images is used to indirectly promotes spatial fiber regularity within neighbor voxels [13]. However, the use of the ℓ_1 norm in the SD context has been shown to be inconsistent with the volume fractions coefficients [14].

In the current work, we leverage both k- and q-space acceleration to recover the FOD coefficients at high spatio-angular resolution. We define the estimated FOD as a solution to a convex regularized minimization problem. Precisely, we use a *structured sparsity* prior promoting simultaneously voxelwise sparsity and spatial smoothness of fiber orientation [15]. The resulting minimization problem is then solved using a forward-backward (FB) algorithm [16]. Results obtained from in vivo data suggest that high spatio-angular resolution FOD mapping can be achieved from severe kq-space acceleration.

The remainder of the paper is organized as follows. The proposed method is described in Section II. In Section III we provide the experimental setup and we present the obtained results. Finally, we conclude in Section IV.

II. Proposed kq-space under-sampling approach

A. Inverse problem

Let N be the number of imaged voxels. The objective is to find an estimate of the unknown FOD field of interest, $X \in \mathbb{R}^{(n+2)\times N}$, from the observation matrix, $\hat{Y} \in \mathbb{C}^{M\times K}$. Each column of X contains the $n+2$ FOD coefficients of the

corresponding voxel. Each row of $\hat{Y}$, denoted by $\hat{Y}_{q,c} \in \mathbb{C}^{1\times K}$, corresponds to the under-sampled k-space of the DW-image acquired with gradient $q \in \{1,\dots,M\}$ and coil receiver $c \in \{1,\dots,C\}$, and is given by:

$$\hat{Y}_q = \mathcal{A}_{q,c}(X) + \eta_{q,c}, \tag{1}$$

where $\eta_{q,c} \in \mathbb{C}^{1\times K}$ is a realization of an i.i.d. Gaussian noise and $\mathcal{A}_{q,c}$ is the linear measurement operator, given by

$$\mathcal{A}_{q,c}(X) = \Phi_q X S_0 H^{(q,c)} U^{(c)} F M^{(q)}. \tag{2}$$

More precisely, $\Phi_q \in \mathbb{R}^{1\times(n+2)}$ is the q^{th} row of the dictionary $\Phi \in \mathbb{R}^{M\times(n+2)}$ that spans the response of a single fiber oriented along n different directions, to which 2 isotropic compartments, representing the gray matter and the cerebrospinal fluid (CSF), are added. The matrix $S_0 \in \mathbb{R}^{N\times N}$ is a diagonal matrix whose elements correspond to the intensities of the image acquired in the absence of diffusion, named $\mathbf{s}_0$ image. Note that S_0 needs to be taken into account in the model for normalization purposes. The diagonal matrix $H^{(q,c)} \in \mathbb{C}^{N\times N}$ is used to account for the phase distortions generated by motion and magnetic field inhomogeneities. The acquisition of the diffusion signal from multiple channels is taken into account through the diagonal matrix $U^{(c)} \in \mathbb{C}^{N\times N}$ which contains the sensitivity map of the corresponding receiver coil c. Finally, $F \in \mathbb{C}^{N\times N}$ represents the 2D Fourier matrix, and $M^{(q)} \in \mathbb{R}^{N\times K^{(q)}}$ is a binary mask that under-samples the slices of the acquired DW volume. The proposed approach is intended to be used with Echo Planar Imaging (EPI), which is the acquisition scheme conventionally adopted for the DW MRI. However, due to calibration purposes, unconventional EPI schemes, performing a non uniform sampling of the k-space lines, are required to be used with the proposed method.

B. Minimization problem

In the context of FODs reconstruction, the signal X is sparse in the q-space as a consequence of the low number of fiber populations (i.e. non-zero FODs coefficients) that are expected to be contained within a voxel. At the imaging resolution available nowadays, it is commonly accepted that no more than five fiber bundles can be distinguished within the same voxel [17]. As a result, only few coefficients, out of all the directions chosen to discretize the sphere, are needed to identify the fiber population contained in each single voxel.

The most suitable way to promote sparsity consists in using the ℓ_0 pseudo-norm [18]. However, this function can be difficult to handle in practice due to its non-smoothness and its non-convexity and it is often replaced by its convex relaxation, the ℓ_1 norm. However, when SD problems are considered, it has been demonstrated that the use of the ℓ_1 norm is inconsistent with the physical constraint that the volume fractions of each voxel sum up to unity [14]. To circumvent this issue, [14] has proposed to use a reweighting ℓ_1 approach [19] to approximate the ℓ_0 pseudo-norm in the context of the voxel-wise FOD estimation. This approach has been subsequently used in the SD framework in [15]. Basically, it consists in solving sequentially several weighted ℓ_1 problems. The weights are chosen to promote simultaneously voxelwise sparsity and spatial smoothness of fiber orientation.

We propose to leverage this reweighted approach to solve the considered general inverse problem (1)-(2). Let $W = (W_{d,v})_{d,v} \in [0,+\infty[^{(n+1)\times N}$ be a weighting matrix. The associated convex minimization problem reads

$$\min_{X\in\mathbb{R}^{(n+2)\times N}} \left\|\mathcal{A}(X) - \hat{Y}\right\|_2^2 \text{ s.t. } X \in \mathcal{B}^+_{1,W}(\kappa), \tag{3}$$

where $\mathcal{A}\colon \mathbb{R}^{(n+2)\times N} \to \mathbb{C}^{MC\times k}$ is the concatenation of the operators $\mathcal{A}_{q,c}$, for all (q,c), and $\mathcal{B}^+_{1,W}(\kappa) = \left\{X \in \mathbb{R}_+^{(n+1)\times N} \,\middle|\, \|X\|_{1,W} \leqslant \kappa\right\}$ is the intersection of the real positive orthant $\mathbb{R}_+^{(n+1)\times N}$ with the weighted ℓ_1 ball of radius $\kappa > 0$, centred in 0. Precisely, $\|X\|_{1,W} = \sum_{v=1}^{N}\sum_{d=1}^{n+1} W_{d,v}|X_{d,v}|$.

C. Reweighted ℓ_1 algorithm for FOD estimation

The proposed global method is described in Algorithm 1. It consists in a reweighting approach, solving problem (3) T times, using different weighting matrices $W^{(t)}$, for $t \in \{0,\dots,T-1\}$, in order to mimic the ℓ_0 pseudo-norm [19].

Algorithm 1 Reweighted FB algorithm for FOD estimation

1: **Input:** Let $X^{(0)} \in {\mathbb{R}_+}^{n+2\times N}$,
2: Let $W^{(0)} \in \mathbb{R}_+^{n+2\times N}$, and $(\kappa,\gamma,\nu) \in]0,\infty[^3$.
3: **Iterations:**
4: **For** $t = 0,1,\dots,T-1$
5: $\quad X^{(t,0)} = X^{(t)}$
6: $\quad$ **for** $j = 0,\dots,J$ `(FB iterations to solve (3))`
7: $\quad\quad \widetilde{X}^{(j+1)} = X^{(j)} - \gamma\mathcal{A}^\dagger\Big(\mathcal{A}(X^{(j)}) - \hat{Y}\Big)$
8: $\quad\quad X^{(t,j+1)} = \mathcal{P}_{\mathcal{B}^+_{1,W^{(t)}}(\kappa)}\Big(\widetilde{X}^{(t,j+1)}\Big)$
9: $\quad\quad$ **If** $\|X^{(j+1)} - X^{(j)}\|_F < \nu\|X^{(j)}\|_F$
10: $\quad\quad\quad$ **Stop**
11: $\quad\quad$ **end if**
12: $\quad$ **end for**
13: $\quad X^{(t+1)} = X^{(t,j+1)}$
14: $\quad$ **Compute** $W^{(t+1)}$ as per equations (4)-(5)
15: $\quad$ **If** $\|X^{(t+1)} - X^{(t)}\|_F < 10^{-3}\|X^{(t+1)}\|_F$
16: $\quad\quad$ **Stop**
17: $\quad$ **end if**
18: **end for**
19: **Output:** $X^\star = X^{(t+1)}$

In each cycle $t \in \{0,\dots,T-1\}$ problem (3) is solved using FB iterations [16]. These sub-iterations are described in lines 6-12 in Algorithm 1. In practice, a maximum number of $J \in \mathbb{N}^*$ inner FB iterations are computed, and the inner-loop is stopped when the stopping criteria given line 9 is satisfied. At each sub-iteration j, $X^{(t,j+1)}$ is updated by performing a gradient step (line 7), followed by a projection step onto the positive weighted ℓ_1 ball, $\mathcal{B}^+_{1,W^{(t)}}(\kappa)$ (line 8). The parameter κ is chosen to represent the X sparsity level.

For every global iteration $t \in \{0, \ldots, T-1\}$, the matrix of weights $W^{(t+1)}$ is updated line 14 of Algorithm 1 using a similar approach as described in [15]. Precisely, we choose

$$W_{d,v}^{(t+1)} = \frac{1}{\tau^{(t+1)} + B_{d,v}^{(t+1)}}, \tag{4}$$

where

$$B_{d,v}^{(t+1)} = \frac{1}{|\mathcal{N}(v)|} \sum_{d'v' \in \mathcal{N}(dv)} |X_{d'v'}^{(t+1)}|, \tag{5}$$

and

$$\begin{cases} \tau^{(0)} = \mathrm{Var}\left(B^{(0)}\right), \\ \tau^{(t+1)} = \max\left\{\frac{\tau^{(t)}}{10}, \overline{\tau}\right\}, \quad (\forall t \in \{0, \ldots, T-1\}) \end{cases} \tag{6}$$

with $\overline{\tau} > 0$. The parameter $\tau^{(t)}$ is a stability parameter that avoids the weights to go to infinity when $B_{d,v}^{(t)} = 0$.

Basically, $B^{(t)}$ is defined as the set of voxels in the support of $X^{(t)}$ that gives a blurred version of $X^{(t)}$.

The *spatial neighborhood* $\mathcal{N}(v)$ is defined as the group of voxels that share either a face, an edge or a vertex with the voxel of interest $v \in \{1, \ldots, N_1\}$. In analogous way, the *angular neighborhood* $\mathcal{N}(d)$ is defined as the set of atoms associated with the directions that fall within a cone of 15° with the direction of interest d. The neighborhood of an element individuated by the indices d and v is then indicated by $\mathcal{N}(dv)$ and corresponds to all the indices in the support of $X^{(t)}$ that are simultaneously included in $\mathcal{N}(v)$ and $\mathcal{N}(d)$.

Weights designed in [15] have a twofold effects. Each element $W_{d,v}^{(t)}$ directly affects the corresponding element $X_{d,v}^{(t+1)}$ in such a way that large weights progressively force to zero spurious peaks, while small weights favor the presence of the FOD coefficients. In this way, the weighting matrix, associated with the ℓ_1 norm, promotes sparsity.

Finally, note that empirical observations suggest to choose $T = 10$ [15], and a stopping criteria is also used to avoid useless re-weighting iterations (line 15).

Once the solution is found, a post-processing procedure is performed along the columns of X to extract the fiber directions within each voxel. We identify the highest peaks among all the directions contained within a cone of 30° for each different direction. No more than 8 local peaks are assumed per voxel and peaks smaller than 20% of the maxima are disregarded to suppress spurious contributions [14], [15].

III. Experimental setup and Results

In this section, we provide simulation results for the fiber configurations recovery problem considering various under-sampling regimes. We consider real DW images acquired on a 3T Magnetom Trio system (Siemens, Germany) with standard clinical protocols. DW volumes consisting of $N = 106 \times 106 \times 51$ voxels have been acquired with $M = 256$ q-points evenly distributed over a single shell, at a b-value of 3000 s/mm^2.

The real DW images have afterwards been manually adapted to model the multi-coil under-sampled kq-space setting. Precisely, the acquisition from 4 coil receivers has been simulated by multiplying each slice of the DW volumes by 4 different sensitivity maps, which have been simulated using the toolbox available at http://bigwww.epfl.ch/algorithms/mri-reconstruction/. In addition, different linear phase maps are multiplied to each slice of the DW volume to simulate the effects produced by motion and magnetic field inhomogeneities. More specifically, the linear phase maps are generated in such a way that the corresponding k-space shift is constrained within 10 phase-encoding lines. The signal so obtained is then converted to k-space through the Fourier transform and selection masks are applied to the k-spaces in order to assess the FOD recovery in the kq-space under-sampling setting described in Section II-A. Results presented in this work have been performed considering k-space under-sampling schemes focusing on the low frequency components of the signal. This scheme can be seen as a super-resolution approach. In addition, to accelerate further the acquisition, we consider also the case when some low frequency lines are skipped, while fully sampling a central region for calibration purposes. An example is shown in Fig. 1 for a low frequency k-space under-sampling factor of 2 (overall k-space under-sampling factor of 3.2 resp.).

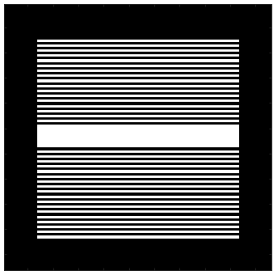

Fig. 1. k-Space under-sampling pattern to evaluate the performance of the proposed method to super-resolve the fiber configurations while accelerating the data acquisition. Scheme corresponding to a low frequency under-sampling factor of 2, which correspond to an overall k-space under-sampling factor of 3.2 (selected points appear in white colour). The k-space consists of 106×106 pixels, the area consisting of 90×90 pixels is considered as low frequency area. The 7 central lines are fully sampled for calibration purposes while the 41 lines above and below the fully sampled region are regularly skipped depending on the low frequency under-sampling factor.

In this work, both the phase and sensitivity maps are unknown. To take them into account in the FOD reconstruction process, we need to estimate them during a pre-processing step (calibration). The phase of each imaged slice is estimated from the central portion of the k-space, which is always fully sampled [20], [21]. Precisely, we compute the inverse Fourier transform of a zero-padded version of the fully sampled central part of the k-space to obtain complex images, the phase of which characterizes the diagonal elements of $H^{(q,c)}$. Images acquired in absence of diffusion from different coil receivers are combined through the *Sum of Squares* method in order to obtain a baseline image [22]. The sensitivity map of each receiver coil is obtained by dividing the image collected with the corresponding coil by the baseline image.

The FOD recovery is performed using the proposed method, with Algorithm 1, where $\kappa = 3N$, and $0 < \gamma < 2/\|\mathcal{A}\|_S^2$. The FOD reconstruction performances are evaluated by taking

into account the mean success rate (SR) and the mean angular error (θ) indices. The mean SR expresses the portion of voxels in which the number of fibers is correctly estimated. When fibers are individuated, (θ) quantifies the angular accuracy with which the fibers orientations are recovered. In addition, we also use a measurement unit called *image unit*. This unit is used to assess the reconstruction performances considering different kq-space under-sampling settings while fixing the total amount of measured samples. More specifically, 1 *image unit* corresponds to the amount of samples that is acquired considering a single diffusion gradient with full k-space. The same *image unit* ratio may result from different q- and k-space under-sampling settings. For example, 30 *image units* can be achieved either by considering 30 q-points with full k-space or 60 q-points with half k-space. Note that the configuration recovered from all the available diffusion gradients (i.e. 256 diffusion gradients) with complete k-space is considered as ground truth and is reported in Fig. 2A as reference.

We provide in Fig. 2 the qualitative and quantitative evaluation of the fiber configurations recovered at different k and q-space under-sampling regimes considering 15 *image units*. The best FOD reconstruction performances are obtained when considering 60 diffusion gradients with a k-space under-sampling factor of 4. The fiber configuration recovered in this setting, reported in Fig. 2E, appears to be very close to the ground truth. The number of fibers passing within each voxel is correctly estimated in 79% of the voxels with a significantly high angular precision ($\theta = 6.45° \pm 0.42°$). When considering a higher number of diffusion gradients at a higher k-space under-sampling rate (Fig. 2B,C and D), the SR index decreases and θ increases, providing fiber configurations that are generally less similar to the ground truth. In parallel, lower FOD reconstruction performances are also achieved when considering a less diffusion gradients at a lower k-space under-sampling rate (Fig. 2F,G and H). In particular, the performances obtained with 15 q-points and full k-space, which correspond to the q-space under-sampling only case, are significantly lower than the ones obtained with 60 diffusion gradients and a k-space under-sampling factor of 4. Thus, by choosing a feasible trade-off between the q-and the k-space under-sampling, complex fiber configurations can be recovered at a quality higher than the one achieved by the state-of-the-art q-space only strategies.

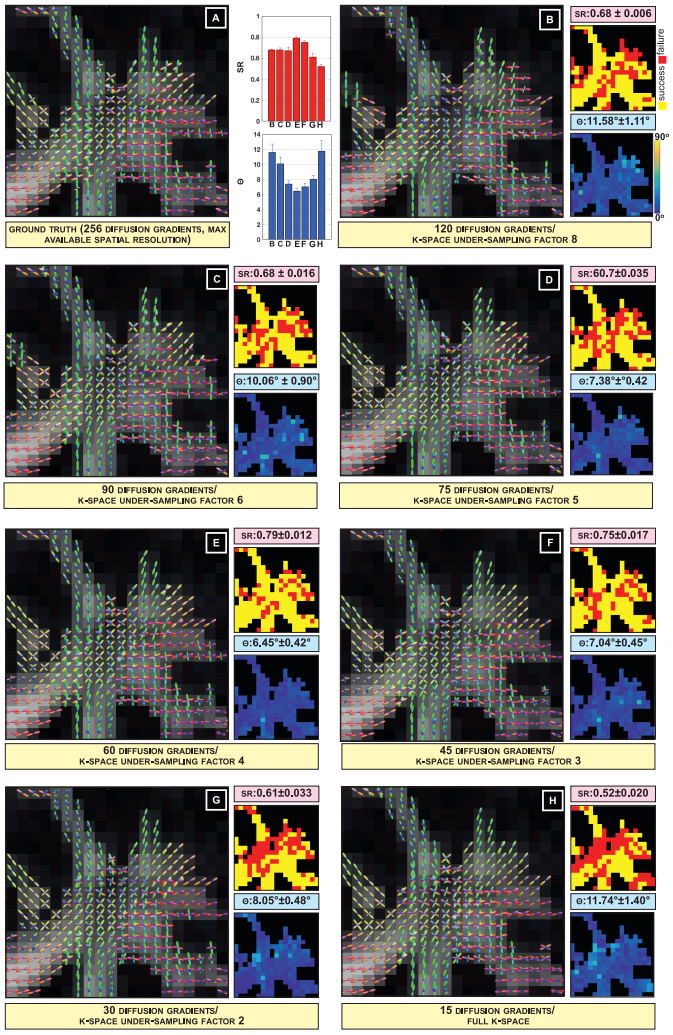

Fig. 2. Qualitative and quantitative evaluation of the fiber configurations recovered from various k and q-space under-sampling regimes by using the proposed framework. (A) Fiber configuration recovered at the maximum available spatial and angular resolution (i.e. full k-space and 256 q-points) representing the ground truth as reference. (B-H) Fiber configurations, success rate (SR) and mean angular error (θ) maps recovered with the proposed method considering different k and q-space regimes, for an overall kq-space sample amount of 15 *image units*.

IV. Conclusion

We developed a method to simultaneously accelerate and super-resolve high angular and spatial resolution dMRI acquisition. We provided a general model to estimate the FODs in presence of multi-coil highly under-sampled kq-space data. The inverse problem is solved leveraging a reweighted ℓ_1 algorithm, based on FB iterations, using the *structured sparsity* prior developed in [15]. The proposed kq-space under-sampling method has been tested on realistic data varying the kq-space under-sampling settings. For a fixed overall under-sampling ratio (*image units*), the proposed approach performs better with moderate under-sampling regimes in both the q-and the k-space, rather than a heavy under-sampling of the signal in only one of the two domains. Typically, fixing the setting to 15 *image units*, the best FOD reconstructions are obtained considering 60 q-points (out of the 256 initially available) with a k-space under-sampling factor of 4. At present, the proposed method has been applied into the general under-sampling setting with EPI schemes which are unconventional for routine acquisitions. However, when applying the method to the super-resolution mode, standard EPI schemes are used. As a result, considering a suitable k and q-space under-sampling trade-off in a general under-sampling mode or in super-resolution setting, the proposed approach enables the accurate recovery of complex fiber architectures within clinically feasible scan times, promoting the application of high spatio-angular resolution dMRI to the clinical setting.

REFERENCES

[1] D. Le Bihan, "Looking into the functional architecture of the brain with diffusion mri," *Nature Reviews Neuroscience*, vol. 4, pp. 469–480, 2003.

[2] O. Sporns, G. Tononi, and R. Kötter, "The human connectome: A structural description of the human brain," *PLoS Computational Biology*, vol. 1, no. 4, pp. 0245–0251, 2005.

[3] Y. Zhang, N. Schuff, A.-T. Du, H. J. Rosen, J. H. Kramer, M. L. Gorno-Tempini, B. L. Miller, and M. W. Weiner, "White matter damage in frontotemporal dementia and Alzheimer's disease measured by diffusion MRI," *Brain*, vol. 132, no. 9, pp. 2579–2592, 2009.

[4] H. J. Park, C. F. Westin, M. Kubicki, S. E. Maier, M. Niznikiewicz, A. Baer, M. Frumin, R. Kikinis, F. A. Jolesz, R. W. McCarley, and M. E. Shenton, "White matter hemisphere asymmetries in healthy subjects and in schizophrenia: A diffusion tensor MRI study," *NeuroImage*, vol. 23, no. 1, pp. 213–223, 2004.

[5] P. J. Basser, J. Mattiello, and D. Le Bihan, "MR Diffusion Tensor Spectroscopy and Imaging," *Biophysical journal*, vol. 66, pp. 259–267, 1994.

[6] J. D. Tournier, F. Calamante, D. G. Gadian, and A. Connelly, "Direct estimation of the fiber orientation density function from diffusion-weighted MRI data using spherical deconvolution," *NeuroImage*, vol. 23, no. 3, pp. 1176–1185, 2004.

[7] J. D. Tournier, F. Calamante, and A. Connelly, "Robust determination of the fibre orientation distribution in diffusion MRI: Non-negativity constrained super-resolved spherical deconvolution," *NeuroImage*, vol. 35, no. 4, pp. 1459–1472, 2007.

[8] B. Jian and B. C. Vemuri, "A unified computational framework for deconvolution to reconstruct multiple fibers from diffusion weighted MRI," *IEEE Transactions on Medical Imaging*, vol. 26, no. 11, pp. 1464–1471, 2007.

[9] D. C. Alexander, "Maximum entropy spherical deconvolution for diffusion MRI." *Information processing in medical imaging*, vol. 19, pp. 76–87, 2005.

[10] F. Dell'Acqua, G. Rizzo, P. Scifo, R. A. Clarke, G. Scotti, and F. Fazio, "A Model-Based Deconvolution Approach to Solve Fiber Crossing in Diffusion-Weighted MR Imaging," *IEEE Transactions on Biomedical Engineering*, vol. 54, no. 3, pp. 462–472, 2007.

[11] A. Ramirez-Manzanares, M. Rivera, B. C. Vemuri, P. Carney, and T. Mareei, "Diffusion basis functions decomposition for estimating white matter intravoxel fiber geometry," *IEEE Transactions on Medical Imaging*, vol. 26, no. 8, pp. 1091–1102, 2007.

[12] M. Lustig, D. Donoho, and J. M. Pauly, "Sparse MRI: The application of compressed sensing for rapid MR imaging," *Magnetic Resonance in Medicine*, vol. 58, no. 6, pp. 1182–1195, 2007.

[13] M. Mani, M. Jacob, A. Guidon, V. Magnotta, and J. Zhong, "Acceleration of high angular and spatial resolution diffusion imaging using compressed sensing with multichannel spiral data," *Magnetic Resonance in Medicine*, vol. 73, no. 1, pp. 126–138, 2015.

[14] A. Daducci, D. Van De Ville, J.-P. Thiran, and Y. Wiaux, "Sparse regularization for fiber odf reconstruction: From the suboptimality of ℓ_2 and ℓ_1 priors to ℓ_0," *Medical Image Analysis*, vol. 18, no. 6, pp. 820–833, 2014.

[15] A. Auría, A. Daducci, J.-P. Thiran, and Y. Wiaux, "Structured sparsity for spatially coherent fibre orientation estimation in diffusion MRI," *NeuroImage*, vol. 115, pp. 245–255, 2015.

[16] P. L. Combettes and V. R. Wajs, "Signal Recovery by Proximal Forward-Backward Splitting," *Multiscale Modeling & Simulation*, vol. 4, no. 4, pp. 1168–1200, 2005.

[17] B. Jeurissen, A. Leemans, J.-D. Tournier, D. K. Jones, and J. Sijbers, "Estimating the number of fiber orientations in diffusion MRI voxels : a constrained spherical deconvolution study," in *International Society of Magnetic Resonance in Medicine 2010*, 2010, p. 573.

[18] D. L. Donoho, "De-Noising by Soft-Thresholding," *IEEE Transactions on Information Theory*, vol. 41, no. 3, pp. 613–627, 1995.

[19] E. J. Candes, M. B. Wakin, and S. P. Boyd, "Enhancing sparsity by reweighted L1 minimisation," *Journal of Fourier Analysis and Applications*, vol. 14, no. 5, pp. 877–905, 2008.

[20] K. L. Miller and J. M. Pauly, "Nonlinear phase correction for navigated diffusion imaging," *Magnetic Resonance in Medicine*, vol. 50, no. 2, pp. 343–353, 2003.

[21] J. G. Pipe, V. G. Farthing, and K. P. Forbes, "Multishot diffusion-weighted FSE using PROPELLER MRI," *Magnetic Resonance in Medicine*, vol. 47, no. 1, pp. 42–52, 2002.

[22] P. B. Roemer, W. A. Edelstein, C. E. Hayes, S. P. Souza, and Muller. O. M., "The NMR Phase Array," *Magnetic Resonance in Medicine*, vol. 16, pp. 192–225, 1990.